

As shown in Figure 8a, comparing to the zero-crossing time of reference current, the zero-crossing time of load current based on FSMPC is delayed by about 45 us, which is expressed as t_n^T , and the zero-crossing time of load current based on FSMPC with delay compensation is delayed by about 35 us, which is denoted as t_n^P . From Figure 8b, average three-phase current residual based on FSMPC is about 1.9 A, current tracking accuracy is 96.8%. Average three-phase current residual based on FSMPC with delay compensation is about 1.3 A, current tracking accuracy is 97.8%. In Figure 8c, the average THD of three-phase reference current is 1.30%, and average THD of three-phase load current based on FSMPC and FSMPC with delay compensation are about 2.4% and 1.80%, respectively. From the Table 5, the sum and average switch power loss based on FSMPC and FSMPC with delay compensation are almost equal.

Table 6. Switch power losses based on FSMPC and FSMPC with delay compensation for low power motor.

	Switch Power Loss (J)						σ (%)
	P_{b1}	P_{b2}	P_{c1}	P_{c2}	P_{sum}	P_{ave}	
FSMPC	41.75	42.16	41.84	40.97	166.72	41.68	0.22
FSMPC with delay compensation	41.80	41.94	41.57	41.06	163.37	41.59	

As shown in Figure 9a, comparing to the zero-crossing time of reference current, the zero-crossing time of load current based on FSMPC is delayed by about 45 us, which is expressed as t_n^T , and the zero-crossing time of load current based on FSMPC with delay compensation is delayed by about 35 us, which is denoted as t_n^P . From Figure 9b, average three-phase current residual based on FSMPC is about 0.17 A, current tracking accuracy is 97.5%. Average three-phase current residual based on FSMPC with delay compensation is about 0.12 A, current tracking accuracy is 98.3%. In Figure 9c, the average THD of three-phase reference current is 2.1%, and average THD of three-phase load current based on FSMPC and FSMPC with delay compensation are about 3.2% and 4.3%, respectively. From the Table 6, the sum and average switch power loss based on FSMPC and FSMPC with delay compensation are almost equal. The experimental results have shown that, for the high and low power motor, the residual between load current and reference current is reduced and current tracking accuracy is improved by applying FSMPC with delay compensation, when compared with FSMPC.

Table 7. Comparison of based on FSMPC and FSMPC with delay compensation for high and low power motor.

	High Power Motor		Low Power Motor	
	FSMPC	FSMPC with Delay Compensation	FSMPC	FSMPC with Delay Compensation
Tracking accuracy of load current	96.8%	97.8%	97.5%	98.3%
Zero-crossing delay time	45 us	35 us	45 us	35 us
THD	2.4%	1.8%	4.3%	3.2%
Decrease percent of switch power loss		0.13%		0.22%
Load inductance		4 mH		0.13 mH
Switching frequency			10 kHz	
Sampling frequency			20 kHz	

4.3. Motor Rotor Broken Bar Fault

When the motor is operating under rotor broken bar fault with the reference current for high power motor set 60 A/20 Hz and low power motor set 7 A/30 Hz respectively, and fault level set 20%. The comparison of current tracking performance and switch power loss for proposed motor emulator without and with power loss minimum control are displayed in this section.

For the high power motor, the experimental waveforms of a -phase reference current, a -phase load current of proposed motor emulator without and with power loss minimization control are shown in Figure 10a. Based on these conditions, the experimental waveforms of average three-phase current residual of between reference current and load current of without and with power loss minimization control are shown in Figure 10b, respectively. The experimental waveforms of average three-phase current THD of reference current, load current with or without power loss minimization control are shown in Figure 10c, respectively. The switch power loss results during entire simulation period of proposed motor emulator without and with power loss minimization control are shown in Table 8. Similarly, the experimental waveforms for the low power motor are shown in Figure 11a–c and Table 9.

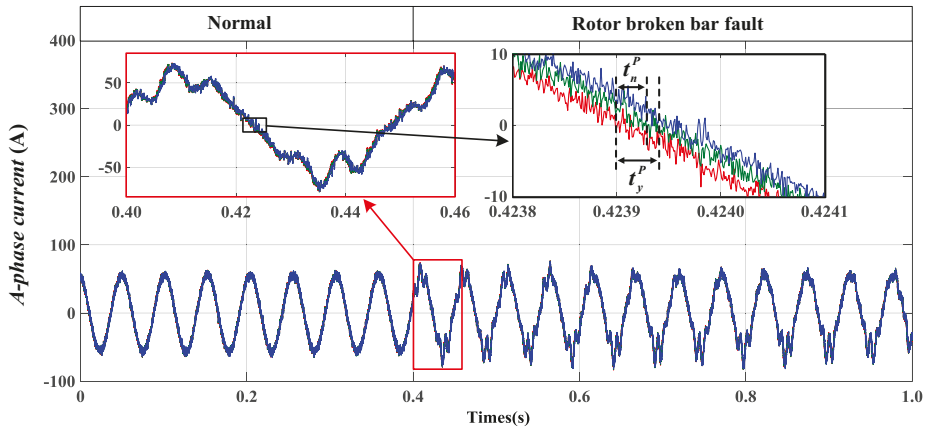
Table 8. Switch power losses of motor rotor broken bar fault for high power motor.

	Switch Power Loss (KJ)						σ (%)
	p_{b1}	p_{b2}	p_{c1}	p_{c2}	p_{sum}	p_{ave}	
Without	22.91	23.84	23.75	22.36	92.86	23.22	22.74
With	17.52	18.37	18.65	17.22	71.76	17.94	

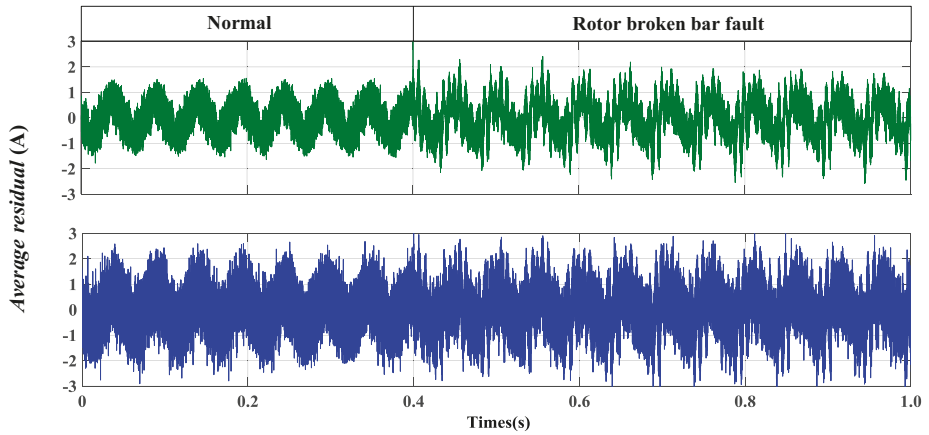
As shown in Figure 10a, when the motor is operating under rotor broken bar fault, comparing to the zero-crossing time of reference current, the zero-crossing time of load current without power loss minimization control is delayed by about 40 us, which is expressed as t_n^p , and the zero-crossing time of load current with power loss minimization control is delayed by about 50 us, which is denoted as t_y^p . From Figure 10b, average three-phase current residual of without and with power loss minimization control are about 2.0 A and 2.2 A, and current tracking accuracy are 96.6% and 96.3%. In Figure 10c, the average THD of three-phase reference current is 19%, and average THD of three-phase load current of without and with power loss minimization control is 22% and 24%, respectively. From Table 8, consideration of power loss, the sum and average switch power loss of the latter have both decreased by 22.74% than the former.

Table 9. Switch power losses of motor rotor broken bar fault for low power motor.

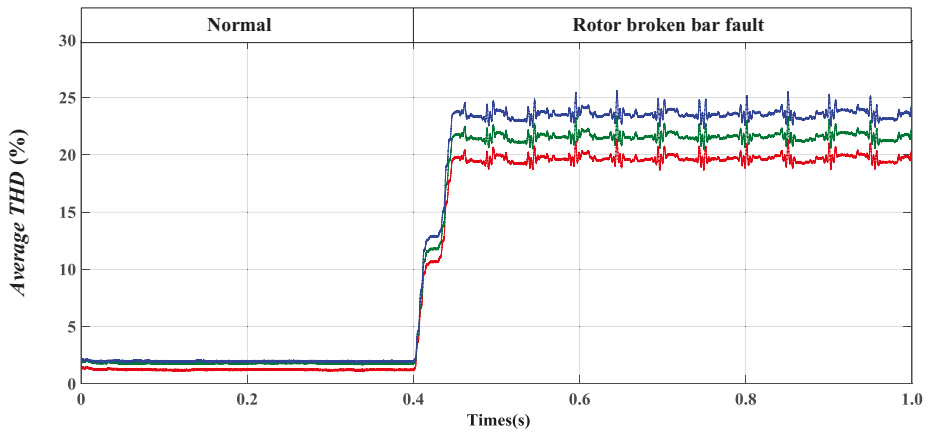
	Switch Power Loss (J)						σ (%)
	p_{b1}	p_{b2}	p_{c1}	p_{c2}	p_{sum}	p_{ave}	
Without	42.29	42.61	41.77	42.85	169.52	42.38	21.47
With	32.96	33.72	33.36	33.04	133.08	33.27	



(a) A-phase currents



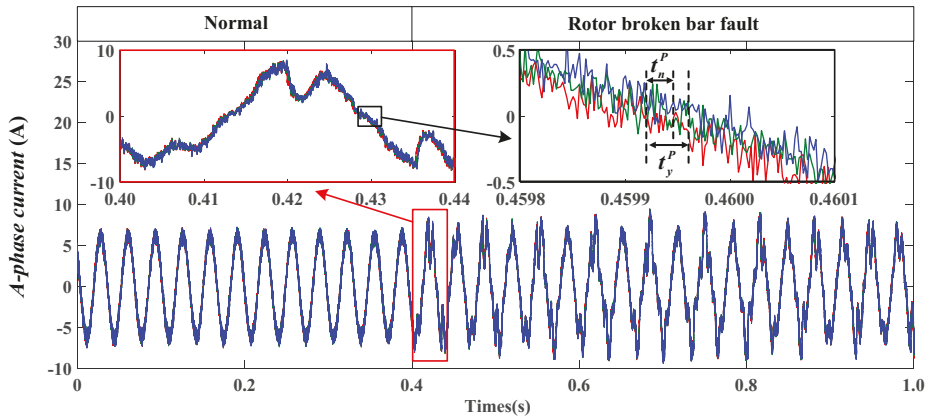
(b) Average residual of three-phase currents



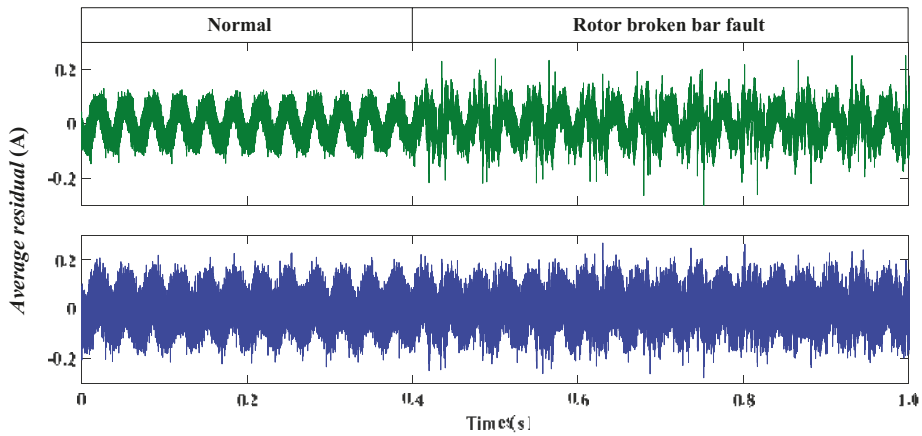
— Reference current
 — Load current of the proposed motor emulator without power loss minimization control
 — Load current of the proposed motor emulator with power loss minimization control

(c) Average THD of three-phase currents

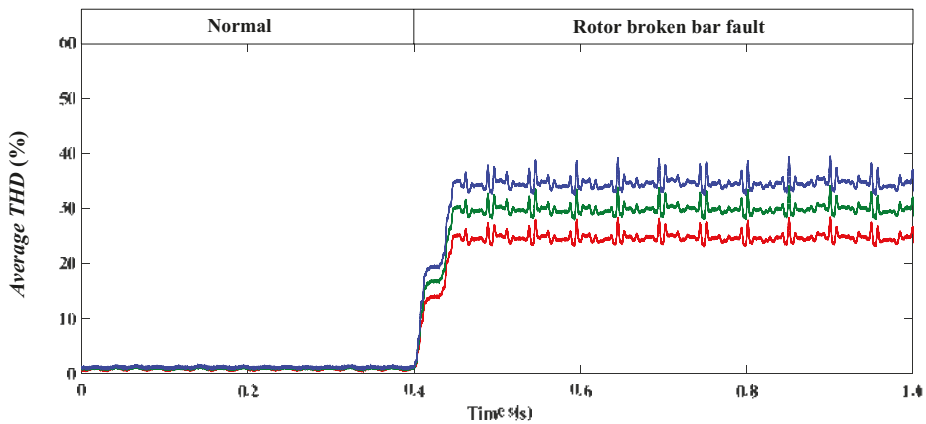
Figure 10. Waveforms of rotor broken bar fault for high power motor.



(a) A-phase currents



(b) Average residual of three-phase currents



- Reference current
- Load current of the proposed motor emulator without power loss minimization control
- Load current of the proposed motor emulator with power loss minimization control

(c) Average THD of three-phase currents

Figure 11. Waveforms of rotor broken bar fault for low power motor.

As shown in Figure 11a, when the motor is operating under rotor broken bar fault, comparing to the zero-crossing time of reference current, the zero-crossing time of load current without power loss minimization control is delayed by about 40 us, which is expressed as t_n^p , and the zero-crossing time of load current with power loss minimization control is delayed by about 50 us, which is denoted as t_y^p . From Figure 11b, average three-phase current residual of without and with power loss minimization control are about 0.15 A and 0.18 A, and current tracking accuracy are 97.8% and 97.4%. In Figure 11c, the average THD of three-phase reference current is 25%, and average THD of three-phase load current of without and with power loss minimization control is 30% and 35%, respectively. From Table 9, consideration of power loss, the sum and average switch power loss of the latter have both decreased by 21.47% than the former, respectively. The experimental results have shown that, for the high and low power motor, the proposed power loss decrease method can reduce effectively switch power loss on the premise of ensuring the current tracking effect of the motor emulator when the motor is operating under rotor broken bar fault.

4.4. Motor Speed Suddenly Alteration

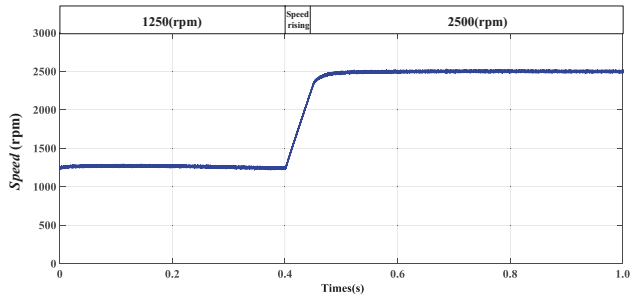
When the motor is operating under speed suddenly alteration with speed set 1250 rpm to 2500 rpm for high power motor and speed set 1000 rpm to 1800 rpm for low power motor respectively, as show in Figures 12a and 13a. The comparison of current tracking performance and switch power loss for proposed motor emulator without and with power loss minimization control are displayed in this section.

For the high power motor, the experimental waveforms of *a*-phase reference current, *a*-phase load current of proposed motor emulator without and with power loss minimization control are shown in Figure 12b. Based on these conditions, the experimental waveforms of average three-phase current residual of between reference current and load current of without and with power loss minimization control are shown in Figure 12c, respectively. The experimental waveforms of average three-phase current THD of reference current, load current of proposed motor emulator without and with power loss minimization control are shown in Figure 12d, respectively. The switch power loss results during the entire simulation period of the proposed motor emulator without and with power loss minimization control are shown in Table 10. Similarly, the experimental waveforms for the low power motor are shown in Figure 13b–d and Table 11.

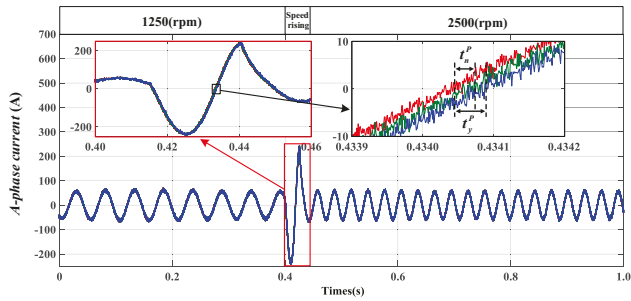
Table 10. Switch power losses of speed suddenly alteration for high power motor.

	Switch Power Loss (KJ)						σ (%)
	P_{b1}	P_{b2}	P_{c1}	P_{c2}	P_{sum}	P_{ave}	
Without	22.76	23.95	23.47	22.36	92.54	23.13	20.83
With	17.72	18.96	18.75	17.83	73.26	18.32	

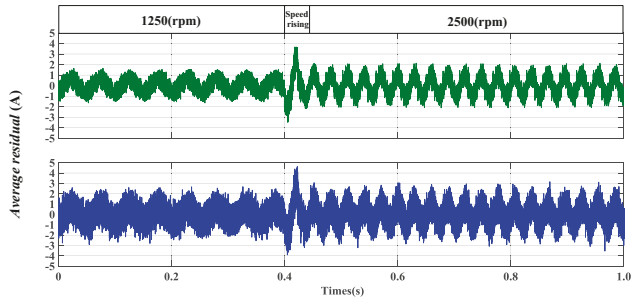
As shown in Figure 12b, when the motor is operating under speed sudden alteration, comparing to the zero-crossing time of reference current, the zero-crossing time of load current without power loss minimization control is delayed by about 40 us, which is expressed as t_n^p , and the zero-crossing time of load current with power loss minimization control is delayed by about 60 us, which is denoted as t_y^p . From Figure 12c, average three-phase current residual of without and with power loss minimization control are about 2.0 A and 2.2 A, and current tracking accuracy are 96.6% and 96.3%. In Figure 12d, the average THD of three-phase reference current is 1.7%, and average THD of three-phase load current of without and with power loss minimization control is 1.9% and 2.0%, respectively. From Table 10, consideration of power loss, the sum and average switch power loss of the latter have both decreased by 20.83% than the former.



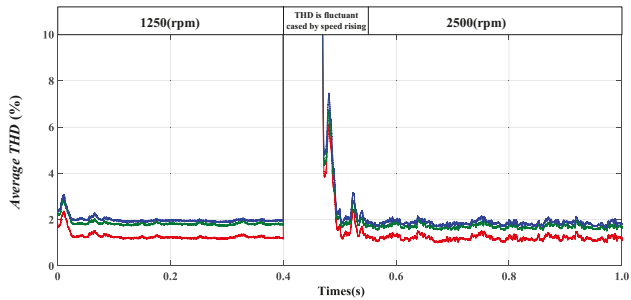
(a) Speed



(b) A-phase currents



(c) Average residual of three-phase currents



— Reference current
 — Load current of the proposed motor emulator without power loss minimization control
 — Load current of the proposed motor emulator with power loss minimization control

(d) Average THD of three-phase currents

Figure 12. Waveforms of speed suddenly alteration for high power motor.

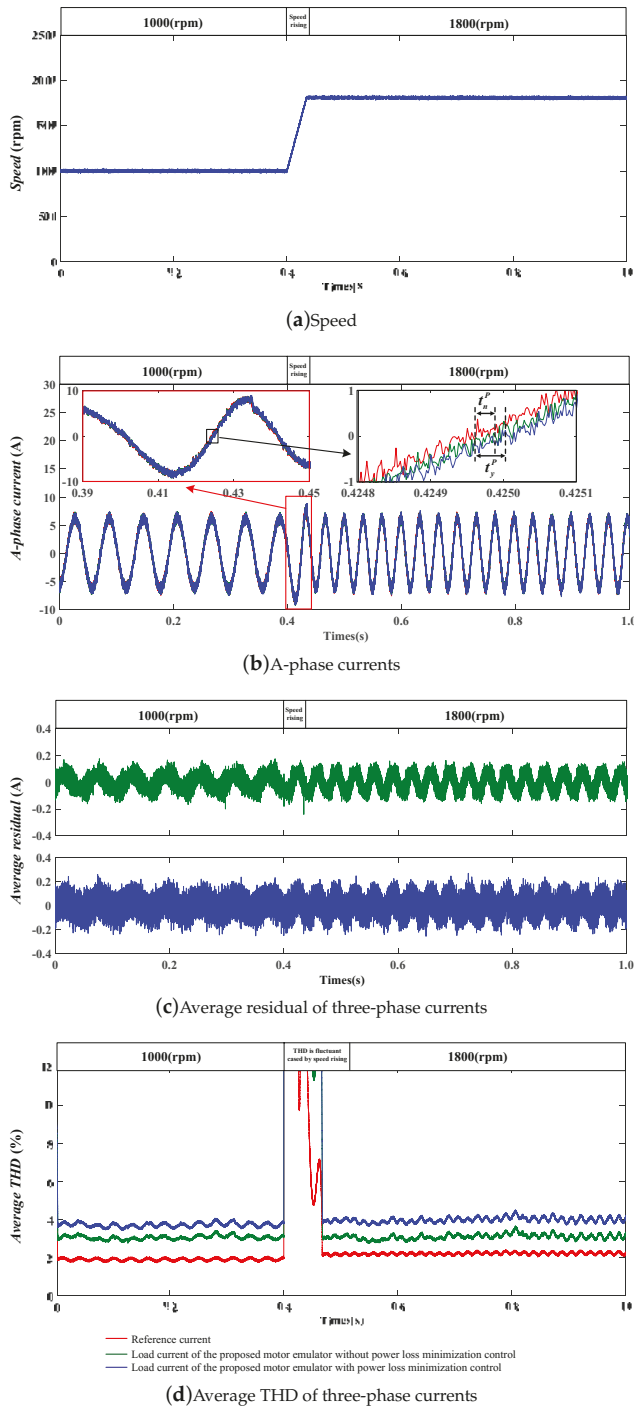


Figure 13. Waveforms of speed suddenly alteration for low power motor.

Table 11. Switch power losses of speed suddenly alteration for low power motor.

	Switch Power Loss (J)						σ (%)
	p_{b1}	p_{b2}	p_{c1}	p_{c2}	p_{sum}	p_{ave}	
Without	45.64	46.32	45.27	45.70	182.94	45.73	20.88
With	36.31	35.97	35.86	36.58	144.72	36.18	

As shown in Figure 13b, when the motor is operating under speed suddenly alteration, comparing to the zero-crossing time of reference current, the zero-crossing time of load current without power loss minimization control is delayed by about 40 μ s, which is expressed as t_n^p , and the zero-crossing time of load current with power loss minimization control is delayed by about 60 μ s, which is denoted as t_y^p . From Figure 13c, average three-phase current residual of without and with power loss minimization control are about 0.16 A and 0.19 A, and current tracking accuracy are 97.7% and 97.3%. In Figure 13d, the average THD of three-phase reference current is 2.0%, and average THD of three-phase load current of without and with power loss minimization control is 3.2% and 4.0%, respectively. From Table 11, consideration of power loss, the sum and average switch power loss of the latter have both decreased by 20.88% than the former, respectively. The experimental results show that, for the high and low power motor, the proposed power loss decrease method can reduce effectively switch power loss on the premise of ensuring the current tracking effect of the motor emulator, when the motor is operating under speed suddenly alteration.

5. Conclusions

A power loss decrease method based on FSMPC with delay compensation for a reduced switch count motor emulator is proposed in this paper. In the proposed motor emulator topology, converter consists of four active switches and two capacitors. Within the power loss decrease method based on FSMPC with delay compensation, an objective function is designed to select the two adjacent switch control signals that generating lowest switch power loss while keeping satisfied current tracking performance. The simulation and experiment results show the feasibility and effectiveness of the proposed method which achieving minimum power loss and ensuring current tracking performance greater than 95%. Besides, they also testify that the current can track stator current accurately and rapidly when the motor operating on the cases, namely in the normal state, or the fault state or the speed suddenly alteration. A real-time platform of a motor emulator for the presented method has been built to provide a reliable environment and offers more authentic data for motor fault injection, diagnosis, and tolerance research.

Author Contributions: conceptualization, R.Q. and C.Y. (Chunhua Yang); methodology, R.Q. and H.T.; software, R.Q.; validation, R.Q. and T.P.; formal analysis, C.Y. (Chunhua Yang); investigation, C.Y. (Chao Yang); resources, C.Y. (Chunhua Yang); data curation, H.T.; writing—original draft preparation, R.Q.; writing—review and editing, C.Y. (Chunhua Yang) and Z.C.; visualization, R.Q.; supervision, Z.C.; project administration, T.P.; funding acquisition, C.Y. (Chao Yang).

Acknowledgments: This research was supported by the National Natural Science Foundation of China (No. 61490702, 61773407, 61621062 and 61803390), by the Key Laboratory of Energy Saving Control and Safety Monitoring for Rail Transportation (No. 2017TP1002), by the Program of the Joint Pre-research Foundation of the Chinese Ministry of Education (No. 6141A02022110), by the General Program of the Equipment Pre-research Field Foundation of China (No. 61400030501), by the Hunan Provincial Innovation Foundation for Postgraduate (No. CX20190064), by the Fundamental Research Funds for the Central Universities of Central South University (No. 2018zzts592).

Conflicts of Interest: The authors declare no conflict of interest.

References

1. Chen, Z.; Li, X.; Yang, C.; Peng, T.; Yang, C.; Karimi, H.R.; Gui, W. A data-driven ground fault detection and isolation method for main circuit in railway electrical traction system. *ISA Trans.* **2019**, *87*, 264–271. [[CrossRef](#)] [[PubMed](#)]
2. Yang, X.; Yang, C.; Peng, T.; Chen, Z.; Liu, B.; Gui, W. Hardware-in-the-Loop Fault Injection for Traction Control System. *IEEE J. Emerg. Sel. Top. Power Electron.* **2018**, *6*, 696–706. [[CrossRef](#)]
3. Chen, Z.; Ding, S.; Peng, T. Fault Detection for Non-Gaussian Processes Using Generalized Canonical Correlation Analysis and Randomized Algorithms. *IEEE Trans. Ind. Electron.* **2018**, *65*, 1559–1567. [[CrossRef](#)]
4. Chen, Z.; Yang, C.; Peng, T.; Dan H.; Li, C.; Gui, W. A Cumulative Canonical Correlation Analysis-Based Sensor Precision Degradation Detection Method. *IEEE Trans. Ind. Electron.* **2019**, *66*, 6321–6330. [[CrossRef](#)]
5. Glowacz, A. Acoustic-Based Fault Diagnosis of Commutator Motor. *Electronics* **2018**, *7*, 299. [[CrossRef](#)]
6. Primavera, S.; Rella, G.; Maddaleno, F. One-cycle controlled three-phase electronic load. *IET Power Electron.* **2012**, *5*, 827–832. [[CrossRef](#)]
7. Tsang, K.M.; Chan, W.L. Fast Acting Regenerative DC Electronic Load Based on a SEPIC Converter. *IEEE Trans. Power Electron.* **2012**, *27*, 269–275. [[CrossRef](#)]
8. Jack, A.G.; Atkinson, D.J.; Slater, H.J. Real-time emulation for power equipment development. Part 1: Real-time simulation. *IEE Proc.-Electr. Power Appl.* **1998**, *145*, 92–97. [[CrossRef](#)]
9. Slater, H.J.; Atkinson, D.J.; Jack, A.G. Real-time emulation for power equipment development. Part 2: The virtual machine. *IEE Proc.-Electr. Power Appl.* **1998**, *145*, 153–158. [[CrossRef](#)]
10. Roodsari, B.N.; Nowicki, E.P. Analysis and Experimental Investigation of the Improved Distributed Electronic Load Controller. *IEEE Trans. Energy Convers.* **2018**, *33*, 905–914. [[CrossRef](#)]
11. Singh, B.; Murthy, S.; Gupta, S. Transient analysis of self-excited induction generator with electronic load controller (ELC) supplying static and dynamic loads *IEEE Trans. Ind. Appl.* **2005**, *41*, 1194–1204. [[CrossRef](#)]
12. Wang, J.; Yang, L.; Ma, Y. Static and Dynamic Power System Load Emulation in a Converter-Based Reconfigurable Power Grid Emulator. *IEEE Trans. Power Electron.* **2016**, *31*, 3239–3251. [[CrossRef](#)]
13. Geng, Z.; Gu, D.; Hong, T. Programmable Electronic AC Load Based on a Hybrid Multilevel Voltage Source Inverter. *IEEE Trans. Ind. Appl.* **2018**, *54*, 5512–5522. [[CrossRef](#)]
14. Heerdt, J.A.; Coutinho, D.F.; Mussa, S.A. Control Strategy for Current Harmonic Programmed AC Active Electronic Power Loads. *IEEE Trans. Ind. Electron.* **2014**, *61*, 3810–3822. [[CrossRef](#)]
15. Kesler, M.; Ozdemir, E.; Kisacikoglu, M.C. Power Converter-Based Three-Phase Nonlinear Load Emulator for a Hardware Testbed System. *IEEE Trans. Power Electron.* **2014**, *29*, 5806–5812. [[CrossRef](#)]
16. Grubic, S.; Amlang, B.; Schumacher, W. A High-Performance Electronic Hardware-in-the-Loop Drive-Load Simulation Using a Linear Inverter (LinVerter). *IEEE Trans. Ind. Electron.* **2010**, *57*, 1208–1216. [[CrossRef](#)]
17. Rao, Y.S.; Chandorkar, M.C. Real-Time Electrical Load Emulator Using Optimal Feedback Control Technique. *IEEE Trans. Ind. Electron.* **2010**, *57*, 1217–1225.
18. Marguc, J.; Truntic, M.; Rodic, M. FPGA Based Real-Time Emulation System for Power Electronics Converters. *Energies* **2019**, *12*, 969. [[CrossRef](#)]
19. Moussa, I.; Khedher, A.; Bouallegue, A. Design of a Low-Cost PV Emulator Applied for PVECS. *Electronics* **2019**, *8*, 232. [[CrossRef](#)]
20. Sadigh, A.; Dargahi, V.; Corzine, K. Investigation of Conduction and Switching Power Losses in Modified Stacked Multicell Converters. *IEEE Trans. Ind. Electron.* **2016**, *63*, 7780–7791. [[CrossRef](#)]
21. Chen, P.; Hu, K.; Lin, Y. Development of a Prime Mover Emulator Using a Permanent-Magnet Synchronous Motor Drive. *IEEE Trans. Power Electron.* **2018**, *33*, 6114–6125. [[CrossRef](#)]
22. Kojabadi, H.M.; Chang, L.C.; Boutot, T. Development of a Novel Wind Turbine Simulator for Wind Energy Conversion Systems Using an Inverter-Controlled Induction Motor. *IEEE Trans. Energy Convers.* **2004**, *19*, 547–552. [[CrossRef](#)]
23. Peng, T.; Liu, B.; Yang, C.; Qin, R.; Yang, C. Fault current tracking method of motor simulator based on finite set model prediction. *J. Cent. South Univ.* **2019**, *50*, 1098–1104.
24. Naderi, Y.; Hosseini, S.; Zadeh, S.; Mohammadi, B.; Savaghebi, M.; Guerrero, J. An optimized direct control method applied to multilevel inverter for microgrid power quality enhancement. *Int. J. Electr. Power Energy Syst.* **2018**, *170*, 496–506. [[CrossRef](#)]

25. Yang, C.; Yang, C.; Peng, T.; Yang X.; Gui, W. A Fault-Injection Strategy for Traction Drive Control System. *IEEE Trans. Ind. Electron.* **2017**, *64*, 5719–5727. [[CrossRef](#)]
26. Chen, X.; Wu, W.; Gao, N.; Liu, J.; Henry S.; Frede B. Finite Control Set Model Predictive Control for an LCL-Filtered Grid-Tied Inverter with Full Status Estimations under Unbalanced Grid Voltage. *Energies* **2019**, *12*, 2691. [[CrossRef](#)]
27. Hu, S.; Liu, G.; Jin, N.; Guo, L. Constant-Frequency Model Predictive Direct Power Control for Fault-Tolerant Bidirectional Voltage-Source Converter with Balanced Capacitor Voltage. *Energies* **2018**, *11*, 2692.



© 2019 by the authors. Licensee MDPI, Basel, Switzerland. This article is an open access article distributed under the terms and conditions of the Creative Commons Attribution (CC BY) license (<http://creativecommons.org/licenses/by/4.0/>).

MDPI
St. Alban-Anlage 66
4052 Basel
Switzerland
Tel. +41 61 683 77 34
Fax +41 61 302 89 18
www.mdpi.com

Energies Editorial Office
E-mail: energies@mdpi.com
www.mdpi.com/journal/energies



MDPI
St. Alban-Anlage 66
4052 Basel
Switzerland

Tel: +41 61 683 77 34
Fax: +41 61 302 89 18

www.mdpi.com



ISBN 978-3-03936-391-9